Nature's Microfluidic Transporter: Rotational Cytoplasmic Streaming at High Péclet Numbers

Jan-Willem van de Meent,[1] Idan Tuval,[1] and Raymond E. Goldstein[1,2]

[1]*Department of Applied Mathematics and Theoretical Physics, Centre for Mathematical Sciences, University of Cambridge, Wilberforce Road, Cambridge CB3 0WA, United Kingdom*

[2]*Cambridge Computational Biology Institute, Centre for Mathematical Sciences, University of Cambridge, Wilberforce Road, Cambridge CB3 0WA, United Kingdom*

(Received 20 June 2008; published 20 October 2008)

Cytoplasmic streaming circulates the contents of large eukaryotic cells, often with complex flow geometries. A largely unanswered question is the significance of these flows for molecular transport and mixing. Motivated by "rotational streaming" in Characean algae, we solve the advection-diffusion dynamics of flow in a cylinder with bidirectional helical forcing at the wall. A circulatory flow transverse to the cylinder's long axis, akin to Dean vortices at finite Reynolds numbers, arises from the chiral geometry. Strongly enhanced lateral transport and longitudinal homogenization occur if the transverse Péclet number is sufficiently large, with scaling laws arising from boundary layers.

DOI: 10.1103/PhysRevLett.101.178102 PACS numbers: 87.16.Wd, 47.61.Ne, 47.63.Jd, 87.19.rh

One of the most striking observations made possible by the invention and refinement of the microscope was reported in 1774 by the Italian physicist Bonaventura Corti [1]. Examining cells of the aquatic plants *Nitella* and *Chara*, he found their fluid contents to be in constant circulation at speeds of fractions of a millimeter per second. This motion, now known as cytoplasmic streaming or cyclosis, was rediscovered by Treviranus [2,3], but not until the work of Kamiya and Kuroda [4] did its origins become clear; cyclosis in plants is driven by the motor protein myosin moving along filamentary actin at the cell periphery [5], carrying cargo [6] that entrains fluid [7].

In the many organisms exhibiting cyclosis, from fungi to amoebae, streaming takes on a great variety of forms. In plants [8,9], there is simple circulation (in the hair cells of *Tradescantia*), fountainlike streaming (in pollen tubes of the lily), and rotational streaming (in *Chara* and *Nitella*), driven by two helical bands of opposite myosin motion. *Chara* grows in branches about 1 mm in diameter, segmented into cylindrical internodal cells several centimeters in size (Fig. 1). One role of streaming may be to facilitate transport between cells by way of nanoscale tubes (plasmodesmata) which connect cells [10]. Streaming may also mix the cellular contents, as would be important for homeostasis [11]. The thin outer layer of cytoplasm in *Chara*, containing the actin-myosin system, is separated from the vacuole by the tonoplast membrane, which regulates the exchange of metabolites with the vacuole [12]. Shear generated in the cytoplasm is transmitted through the tonoplast, yielding flows throughout the vacuole [4,13].

Quite apart from implications of streaming for cellular metabolism [14], the advection-diffusion problem presented by Characean algae holds considerable intrinsic interest as a form of Stokes flow not previously examined. The speed U of streaming can reach 100 μm/s in a cell of radius R as large as 0.5 mm, so for even the smallest molecular species, with diffusion constant $D \sim 10^{-5}$ cm^2/s, the Péclet number $\mathrm{Pe} = UR/D$ can be 10^2–10^3. Thus, advection strongly dominates diffusion even though the Reynolds number $\mathrm{Re} = UR/\nu$ is small. Here, we show that the combination of helical forcing [Fig. 1(b)] and high Péclet numbers in what we term "Nature's microfluidic transporter," found by evolution more than 500 million years ago, can lead to intriguing properties: (i) fast radial mass redistribution, (ii) enhanced mass flux across the boundary of the cell, and (iii) homogenization of longitudinal advection. These arise from the generation of transverse flows [Fig. 1(c)] akin to Dean vortices in curved pipes [15], which can promote mixing in various contexts [16]. While Dean vortices appear at finite Re, the streaming flows are found at $\mathrm{Re} = 0$. The regime $\mathrm{Pe} \gg 1$ is associated with boundary layers that

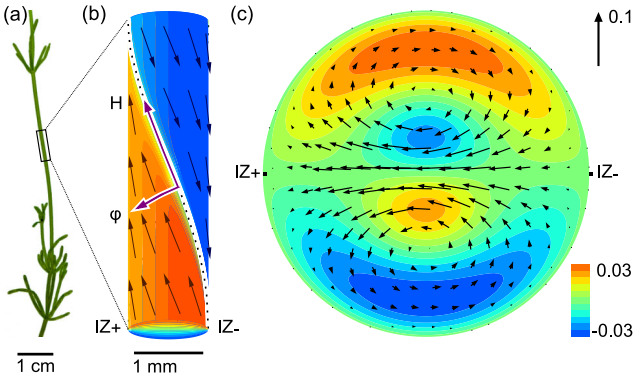

FIG. 1 (color online). The plant *Chara corallina*. (a) Portion of a specimen of *C. corallina* v. australis, courtesy of Botanic Garden, University of Cambridge. (b) Velocity boundary conditions and indifferent zones $\mathrm{IZ}_{\pm}$. (c) Velocity fields; colors/intensities denote component along H-axis and arrows represent projections of radial velocity in the plane.

enhance transport, to a degree that depends on specifics of boundary conditions at surfaces [17–20].

In microfluidic lab-on-a-chip technologies [21], the achievement of rapid and efficient mixing is a key challenge. Solutions range from static multilayer lamination [22,23] and hydrodynamic focusing [24] to mixers that exploit the chaotic advection paradigm to increase the interfacial contact area across which diffusion acts [25,26]. New microfluidic methods exploiting the rotational streaming paradigm may be of significant interest.

Stripping away biological complexities (tonoplast, distinction between cytoplasm and vacuole [27]), we study the dimensionless geometry of Fig. 1(b), a cylinder of radius 1, whose inner surface has "barber-pole" velocity boundary conditions: piecewise constant (with values ± 1) along two helical bands of wavelength λ. The two divisions between these bands are known as indifferent zones (IZ), labeled "$\pm$" according to whether the nearby transverse flow is into or out of the cylinder center. Streaming rates become independent of cell length l for $l \gtrsim 5$ [28], so we let $l \to \infty$ and discard possible 3D effects introduced at the cell ends for simplicity. We seek solutions of the Stokes equation, $\eta \nabla^2 \mathbf{u} = \nabla p$, for an incompressible velocity $\mathbf{u}$ of a Newtonian fluid with pressure p.

For any finite λ, the helical symmetry implies invariance up to a rotation $2\pi z/\lambda$. Natural coordinates are (r, φ), where $\varphi = \theta - \kappa z$ is the helical angle and $\kappa = 2\pi/\lambda$ is the spiral wave number. A unique basis is the radial unit vector, $\mathbf{e}_r$, $\mathbf{e}_\varphi = \nabla\varphi/|\nabla\varphi|$, and $\mathbf{e}_H = \mathbf{e}_r \times \mathbf{e}_\varphi$, or

$$\mathbf{e}_\varphi = \frac{1}{h}(\mathbf{e}_\theta - \kappa r \mathbf{e}_z), \qquad \mathbf{e}_H = \frac{1}{h}(\kappa r \mathbf{e}_\theta + \mathbf{e}_z), \tag{1}$$

where $h = \sqrt{1 + \kappa^2 r^2}$. We set the H-dependence in the metric by the constraint $\Delta\varphi \Delta H \propto r$; a surface of constant r, with area $2\pi r L$, maps to a fixed interval in φ and H. Then the line element is

$$ds^2 = dr^2 + \frac{r^2}{h^2} d\varphi^2 + h^2 dH^2. \tag{2}$$

In an infinite cylinder, with the flow invariant along H, the continuity equation simplifies to $r[\partial_r(r u_r) + h \partial_\varphi u_\varphi] = 0$. This is satisfied by introducing a stream function $\Psi(r, \varphi)$, with $u_r(r, \varphi) = -(1/r)\partial_\varphi \Psi$, and $u_\varphi(r, \varphi) = (1/h)\partial_r \Psi$, so

$$\mathbf{u} = v(r, \varphi)\mathbf{e}_H - \frac{1}{h}\nabla\Psi(r, \varphi) \times \mathbf{e}_H. \tag{3}$$

When $\lambda \to \infty$, we have $\mathbf{e}_H \to \mathbf{e}_z$ and $\Psi \to 0$, reflecting a symmetry $\mathbf{u}(r, \theta) = -\mathbf{u}(r, -\theta)$. The solution is [13] $v(r, \theta) = (2/\pi)\arctan[2r\sin\theta/(1 - r^2)]$. For λ finite, this symmetry is broken by the chirality of the helical trajectories, for the geometry in Fig. 1(b) is left-handed; both upward and downward bands perform a counterclockwise spiral along the direction of motion. With this reduced symmetry, Ψ need not vanish, and the periodicity in φ allows a Fourier expansion,

$$\Psi(r, \varphi) = \sum_{n \text{ odd}} \psi_n(r) \sin n\varphi. \tag{4}$$

A solution of the flow field is obtained by expanding the radial modes of v and Ψ in modified Bessel functions [14,29], whose properties imply that the stream function is dominated by the first mode, and thus

$$u_r \simeq -\frac{\psi_1(r)}{r}\cos\varphi, \qquad u_\varphi \simeq \frac{\psi_1'(r)}{h}\sin\varphi. \tag{5}$$

Figure 2(a) shows that the form of $\psi_1(r)$ is largely insensitive to λ, apart from a scalar amplitude $\alpha(\lambda)$. This mode is a simple symmetry-breaking perturbation of the downstream flow and is well-represented by [30]

$$\psi_1(r) \simeq \alpha r(1 - r^2)^2. \tag{6}$$

At the wavelength $\lambda_{\max} = 2.8$ that maximizes transverse flow, the amplitude is $\alpha = 0.06$ [Fig. 2(a)]. It decreases for shorter λ, where the forcing from narrow helical bands is inefficient, and also for larger wavelengths, on approach to the axially symmetric case.

Since advective trajectories follow level lines of the stream function, the maximum of $\psi_1(r)$ at $r = 1/\sqrt{5}$ defines extrema at $\varphi = \pm\pi/2$ that are the centers of a double vortex. In a Poincaré projection [Fig. 2(b)], this periodic flow is seen to be greatest along the line connecting the IZ, where the downstream flow vanishes. Although appropriately selected perturbations could, in principle, lead to chaotic trajectories, those found *in vivo* (i.e., spatial variations in helical pitch and end effects) seem not to be significant enough for that to be the case. However, two key results emerge solely from these streamline properties: material is rapidly carried between the IZ, crossing the cell in 0.5–1 helical periods, and the average downstream displacement is homogenized by exchange of material between the stagnant central region and the high (longitudinal) speed regions at the periphery.

Consider next the consequences of this complex flow field on a molecular solute whose concentration C obeys

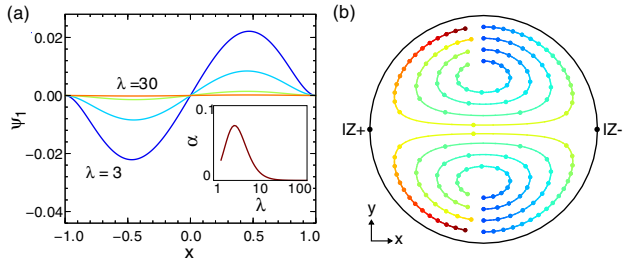

FIG. 2 (color online). Rotational streaming flow. (a) Lowest-order stream function ψ_1 along transverse slice of cylinder, at various wavelengths λ. Inset shows prefactor α [Eq. (6)]. (b) Poincaré plot at $\lambda = 3.0$, with colors/intensities indicating displacement along the z-axis, and markers denote a z-displacement of $\lambda/4$.

the advection-diffusion equation,

$$C_t + Pe\mathbf{u} \cdot \boldsymbol{\nabla} C = \nabla^2 C, \tag{7}$$

where the advective term partitions into downstream and "mixing" components, which couple to v and Ψ,

$$\mathbf{u} \cdot \boldsymbol{\nabla} C = v\partial_H C - \frac{1}{r}\partial_\varphi \Psi \partial_r C + \frac{1}{h}\partial_r \Psi \partial_\varphi C. \tag{8}$$

In a problem where the concentration is also invariant along H, it is then natural to define the transverse Péclet number $\mathrm{Pe}^* = \alpha \mathrm{Pe}$. Inspired by the vacuole's roles as both storage facility and metabolic buffer for cytoplasmic processes, we examine the effect of streaming on the reequilibration of a well-mixed system in response to a jump in the concentration at the boundary.

Figure 3 displays the results of numerical studies (with methods given elsewhere [14]). For finite λ, the broken symmetry of the flow produces an asymmetric concentration field exhibiting a steep gradient of C at the cylinder wall near IZ_+ and a tongue with moderate slope crossing the cylinder from IZ_-. The net effect is an enhanced total flux and decrease in the time for reequilibration. In a section of $C(x, t)$ along $y = 0$ in Fig. 3(a), we define the normalized concentration profile $\Delta(x, t) \equiv (C - C_{\min})/(1 - C_{\min})$ [Fig. 3(b)], where $C_{\min} = C(x_{\min}, t)$ is the minimum concentration. The boundary layer thickness ϵ may be calculated as $\epsilon = \int_{-1}^{x_{\min}} \Delta(x, t) dx$. For large t (but before the advancing tongue fully crosses the cylinder), ϵ converges to a constant that decreases with Pe^* [Fig. 3(c)].

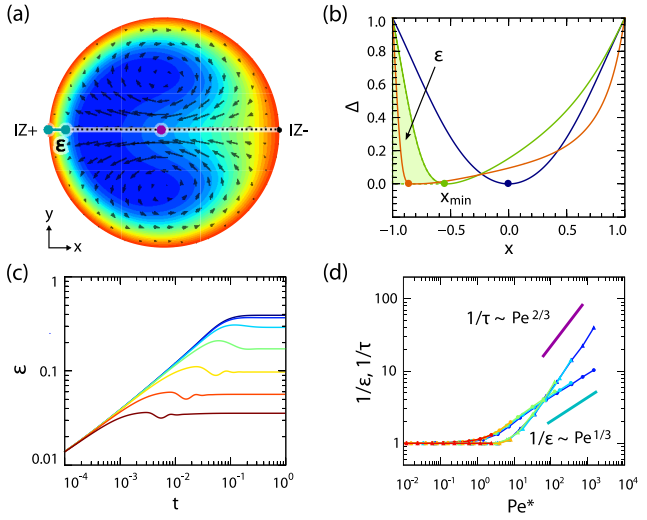

FIG. 3 (color online). Advection-diffusion dynamics. (a) Snapshot of concentration and flow (arrows). (b) Rescaled concentration along the diameter connecting $\mathrm{IZ}_\pm$ in (a), for $\lambda = 3.0$ and $\mathrm{Pe} = 0, 500, 10^4$. (c) Boundary layer scale near IZ_+ vs time for $\mathrm{Pe} = 0,\ 10,\ 50,\ 200,\ 10^3,\ 5 \times 10^3,\ 2 \times 10^4$. (d) Scaling of boundary layer gradient $1/\epsilon$ and tongue propagation rate $1/\tau$ with Pe^*. Colors/intensities denote results with $\lambda = 3.0, 5.7, 12, 25, 47$.

The scaling of ϵ with Pe follows from a dominant balance argument in a local Cartesian coordinate system near the stagnation point IZ_+. Let $s = 1 - r \ll 1$ be the distance from the wall and $\chi = \varphi - \pi \ll 1$ the angular distance from IZ_+. For a quasi-steady-state profile $C = F(S)$, where $S = s/\epsilon$, the flow components are $u_s \propto -\frac{1}{2}s^2$ and $u_\chi \propto s\chi$. The dominant terms in (7) are

$$0 \simeq \tfrac{1}{2}\mathrm{Pe}^* \epsilon S^2 F'(S) + \frac{1}{\epsilon^2} F''(S). \tag{9}$$

Balancing these terms yields the familiar [17] boundary layer scale $\epsilon \propto \mathrm{Pe}^{*-1/3}$, as in Fig. 3(d). The time for development of the boundary layer is estimated from the mean concentration $\bar{C} = (1/\pi) \iint_{\mathcal{D}} dr d\varphi r C(r, \varphi, t)$, where the domain $\mathcal{D}$ is that of the boundary layer. Assuming a self-similar form, $\bar{C}(t) \sim \epsilon G(t/\tau)$, then $d\bar{C}/dt \sim (\epsilon/\tau) G'(t/\tau)$. Mass conservation further relates $d\bar{C}/dt$ and the boundary flux. In dimensionless form,

$$\frac{d}{dt}\bar{C}(t) \sim -\frac{1}{\pi}\int d\varphi\, \partial_r C(r, \varphi, t) \sim \frac{1}{\epsilon}, \tag{10}$$

so $\epsilon/\tau \sim 1/\epsilon$ and $\tau \propto \epsilon^2 \propto \mathrm{Pe}^{*-2/3}$, as in Fig. 3(d).

While enhanced fluxes imply fast radial mass transport, a different metric is required to determine the role of vorticity in downstream transport. Axially symmetric pressure-driven flows may exhibit Taylor diffusion [31]; a parabolically-deforming sheet of solute redistributes radially by diffusion, producing for $t \gg \mathrm{Pe}$ a self-similar concentration profile moving at the mean velocity and spreading longitudinally with an effective diffusivity $\sim \mathrm{Pe}^2$. This phenomenon persists in the presence of transverse circulation, which results in a lowered effective diffusivity [32] and shorter time scale for convergence to the Taylor dispersion limit, as in the case of the staggered herringbone micromixer [25].

The Taylor diffusion approximation will not necessarily hold for the comparatively short Characean internodal cells, whose aspect ratio ($\sim 10^2$) implies that the longitudinal advection time L/U is comparable to the radial diffusion time R^2/D. Even on such intermediate time scales, z-displacements are homogenized as fluid parcels are advected along vortex loops in the $r\varphi$-plane.

We quantify this homogenization by the time-dependent variation in z-displacements for a set of points initially in a sheet at $z = 0$. Figure 4(a) shows the standard deviation $\sigma = (\overline{z^2} - \bar{z}^2)^{1/2}$ of z-displacements relative to the mean $\bar{z}$, which decreases to zero over a time $\sim 1/\alpha$ as z-displacements are averaged out by the circulation. The absolute magnitude of σ [Fig. 4(a), inset] shows a logarithmic dependence that levels off as the grid resolution of the trajectories becomes insufficient to continuously represent the diverging circulation time at the wall. The typical loop time τ_{loop} over which $\sigma/\bar{z}$ falls off to half its initial value defines a typical length $\xi = \tau_{\mathrm{loop}} \bar{u}_z$ over which z-displacements homogenize. The dependence of ξ on λ

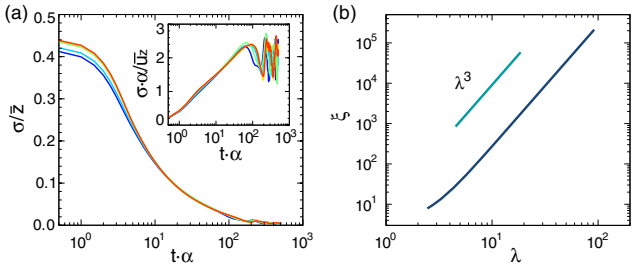

FIG. 4 (color online). Homogenization of downstream transport. (a) Relative standard deviation of z-displacements tends to zero in a time $\propto 1/\alpha$ due to logarithmic growth of the absolute standard deviation (inset). Curves of different colors show a collapse of datasets with $\lambda = 3.0, 5.7, 12, 25, 47$. (b) The length ξ over which the z-displacements homogenize scales as $\bar{u}_z/\alpha$, showing a λ^3 dependence as the circulation decreases to zero.

[Fig. 4(b)] is dominated by a $1/\alpha$ dependence, leading to a very strong λ^3 scaling as the amplitude of the stream function approaches zero.

To summarize, breaking the symmetry via chiral wall forcing leads to some remarkable transport properties: enhanced mass flux across the boundary, fast radial redistribution, and short longitudinal homogenization lengths. The generation of secondary flows analogous to Dean vortices at zero Reynolds number (generated by actin-myosin coupling in *Chara*), could be implemented by, for instance, electro-osmotic flows for microfluidic applications. Techniques for pattering of charged surfaces [33] and/or the control of the electro-osmotic flow by light [34] serve as proof-of-principle for the creation of spatially complex forcing at the microchannel wall. At the considered length scales, the time for diffusive transport becomes prohibitively expensive and fast and efficient advection–mediated homogenization is key. That would seem to be also the case for the Characean algae. A previously-noted relationship between the spiral wavelength and cell growth rate in *Nitella* [14] may be evidence of this, as is the role of streaming in tip-growth of fungi. Indeed, the ubiquity of streaming in its diverse forms emphasizes the relevance of fluid dynamics for intracellular processes.

We thank D. F. Mandoli, J. Mestel, T. J. Pedley, M. Polin, and W. van Saarloos for discussions. This work was supported by the EPSRC and the University of Leiden (J.-W. vdM.), the Human Frontier Science Program (I. T.), DOE Grant DE-AC02-06CH11357, the Leverhulme Trust, and the Schlumberger Chair Fund (R. E. G.).

[1] B. Corti, *Osservazione Microscopische sulla Tremella e sulla Circulazione del Fluido in Una Planto Acquaguola* (Appresso Giuseppe Rocchi, Lucca, Italy, 1774).
[2] L. C. Treviranus, *Beyträge zur Pflanzenphysiologie* (Dieterich, Göttingen, 1811).
[3] A. Hughes, *A History of Cytology* (Abelard-Schuman, London, 1959).
[4] N. Kamiya and K. Kuroda, Bot. Mag. Tokyo **69**, 544 (1956).
[5] T. Shimmen, Journal of Plant Research **120**, 31 (2007).
[6] B. Kachar, Science **227**, 1355 (1985).
[7] D. Houtman *et al.*, Europhys. Lett. **78**, 18001 (2007).
[8] N. Kamiya, *Protoplasmic Streaming* (Springer-Verlag, Vienna, 1959).
[9] N. S. Allen and R. D. Allen, Annu Rev Biophys Bioeng **7**, 497 (1978).
[10] W. F. Pickard, Plant, Cell and Environment **26**, 1 (2003).
[11] P. W. Hochachka, Proc. Natl. Acad. Sci. U.S.A. **96**, 12233 (1999).
[12] E. Martinoia, M. Maeshima, and H. E. Neuhaus, Journal of Experimental Botany **58**, 83 (2007).
[13] W. F. Pickard, Canadian Journal of Botany (1951-) / Journal Canadien de Botanique **50**, 703 (1972).
[14] R. E. Goldstein, I. Tuval, and J. W. van de Meent, Proc. Natl. Acad. Sci. U.S.A. **105**, 3663 (2008).
[15] W. R. Dean, Proc. R. Soc. A **121**, 402 (1928).
[16] S. A. Berger, L. Talbot, and L.-S. Yao, Annu. Rev. Fluid Mech. **15**, 461 (1983).
[17] M. A. Lévêque, Annales des mines **13**, 201 (1928).
[18] A. Acrivos and T. D. Taylor, Phys. Fluids **5**, 387 (1962).
[19] V. Magar, T. Goto, and T. J. Pedley, Q. J. Mech. Appl. Math. **56**, 65 (2003).
[20] M. B. Short *et al.*, Proc. Natl. Acad. Sci. U.S.A. **103**, 8315 (2006).
[21] J. P. Brody, P. Yager, R. E. Goldstein, and R. H. Austin, Biophys. J. **71**, 3430 (1996).
[22] V. Hessel, H. Lowe, and F. Schonfeld, Chem. Eng. Sci. **60**, 2479 (2005).
[23] F. G. Bessoth, A. J. deMello, and A. Manz, Anal. Commun. **36**, 213 (1999).
[24] J. B. Knight, A. Vishwanath, J. P. Brody, and R. H. Austin, Phys. Rev. Lett. **80**, 3863 (1998).
[25] A. D. Stroock *et al.*, Science **295**, 647 (2002).
[26] F. Bottausci, C. Cardonne, C. Meinhart, and I. Mezic, Lab Chip **7**, 396 (2007).
[27] E. A. Nothnagel and W. W. Webb, J. Cell Biol. **94**, 444 (1982).
[28] W. F. Pickard, Protoplasma **82**, 321 (1974).
[29] V. V. Meleshko, V. S. Malyuga, and A. M. Gomilko, Proc. R. Soc. A **456**, 1741 (2000).
[30] The magnitude of the normalized error $|\psi_1(r)/\psi_1'(0) - r(1-r^2)^2|$ is $\mathcal{O}(3\times10^{-2})$ at $\lambda = \lambda_{\max}$ and drops off to $\mathcal{O}(3\times10^{-5})$ at $\lambda = 10\lambda_{\max}$.
[31] G. I. Taylor, Proc. R. Soc. A **219**, 186 (1953).
[32] B. E. Erdogan and P. C. Chatwin, J. Fluid Mech. **29**, 465 (1967).
[33] C. C. Chang and R. J. Yang, J. Micromech. Microeng. **16**, 1453 (2006).
[34] L. Oroszi, A. Dér, H. Kirei, P. Ormos, and V. Rakovics, Appl. Phys. Lett. **89**, 263508 (2006).